Journal of Colloid and Interface Science 632 (2023) 260–270

Contents lists available at ScienceDirect

Journal of Colloid and Interface Science

journal homepage: www.elsevier.com/locate/jcis

Molecular orientation rules the efficiency of immobilized antioxidants

Adél Szerlauth [a,b], Zsuzsanna D. Kónya [b], Gréta Papp [b], Zoltán Kónya [c], Ákos Kukovecz [c], Márton Szabados [d,e], Gábor Varga [a,*], István Szilágyi [a,b,*]

[a] Department of Physical Chemistry and Materials Science, University of Szeged, H-6720 Szeged, Rerrich Béla tér 1, Hungary
[b] MTA-SZTE Lendület Biocolloids Research Group, University of Szeged, H-6720 Szeged, Rerrich Béla tér 1, Hungary
[c] Department of Applied and Environmental Chemistry, University of Szeged, H-6720 Szeged, Rerrich Béla tér 1, Hungary
[d] Department of Organic Chemistry, University of Szeged, Dóm tér 8, Szeged H-6720, Hungary
[e] Material and Solution Structure Research Group, Institute of Chemistry, University of Szeged, Aradi vértanúk tere 1, Szeged H-6720, Hungary

GRAPHICAL ABSTRACT

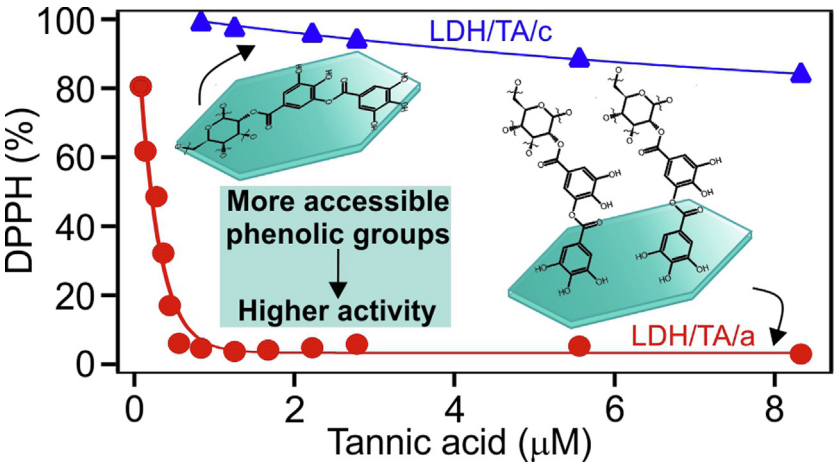

ARTICLE INFO

Article history:
Received 28 August 2022
Revised 1 November 2022
Accepted 11 November 2022
Available online 15 November 2022

Keywords:
Layered double hydroxide
Tannic acid
Glutathione
Structure-activity relationship
Interlamellar expansion

ABSTRACT

Tannic acid (TA) and glutathione (GSH) are important molecular antioxidants against reactive oxygen species. Their efficiency is limited by low solubility and high sensitivity, which may be solved by confinement in composite materials. Here, effect of immobilization of these antioxidants on their radical scavenging activity was investigated using layered double hydroxide (LDH) nanoparticles as hosts. Different preparation methods were applied to build composite systems leading to variations in the molecular orientation of both TA and GSH on the surface or among the layers of LDHs. Systematic combination of spectroscopy (FT-IR, Raman, UV–VIS-NIR-DRS), diffraction (XRD) and microscopy (SEM) methods revealed perpendicular or parallel orientation of TA on the surface of LDH depending on the preparation approach applied. Immobilization of GSH protected the antioxidant molecules from degradation. Radical scavenging tests evidenced that the activity of the antioxidants strongly depends on the molecular orientation. The LDH supported GSH and TA proved as durable and reusable antioxidant agents to be applied as radical scavengers in medical therapies or in industrial processes.

* Corresponding authors at: Department of Physical Chemistry and Materials Science, University of Szeged, H-6720 Szeged, Rerrich Béla tér 1, Hungary (G. Varga and I. Szilágyi).
E-mail addresses: gabor.varga5@chem.u-szeged.hu (G. Varga), szistvan@chem.u-szeged.hu (I. Szilágyi).

https://doi.org/10.1016/j.jcis.2022.11.056
0021-9797/

1. Introduction

Industrial applications of antioxidants have already evolved since the late 60′s, when the essential role of the native enzymes in the defence system of the human body against reactive oxygen species (ROS) and reactive nitrogen species (RNS) was demonstrated [1]. Thereafter, antioxidant-based processes have become indispensable for various industries – such as food or cosmetic manufacturing – to reduce the amounts of by-products, to extend expiration-date and, in parallel, to maximize the economic profit [2–5].

More recently, natural exogenous antioxidants are being increasingly used as functional scavengers [6–11]. For instance, they reduce hydroperoxides to harmless alcohols during polymer stabilizing processes [12,13] allowing the substitution of the health risky alkylphenols, which are often used as secondary stabilizers [14,15]. One of the most auspicious antioxidant family is the polyphenols including lignin and tannic acid (TA) with remarkable long-term activity, biocompatibility and stability. However, their efficiency cannot be fully exploited, because a large portion of the phenolic groups are hidden within the molecules leading to limited accessibility to ROS [12]. Thiolate/disulphide-based antioxidants are not tested in such industrial processes owing to their sensitive structure and consequently, to their difficult long-term storage [16,17].

Among various antioxidants, native enzymes are still the most widely used materials in both medical and industrial applications [18,19]. Despite their indisputable advantages, such as substrate specificity and high catalytic turnover number, the enzyme-involved processes are strongly limited to a narrow range of the reaction conditions to ensure the structural integrity and activity of the proteins [20]. Moreover, the optimal conditions are difficult to overlap with those ones generally required for industrial manufacturing [21]. In contrast, other non-enzymatic antioxidants would be capable to function under more extended reaction conditions [22]. However, because of their numerous disadvantages ranging from the non-biocompatible feature to the reduced solubility, the use of non-enzymatic natural antioxidants have significantly diminished [23].

To eliminate these drawbacks, numerous immobilization methods have been designed and developed for enzymatic and non-enzymatic antioxidants. Concerning solid support, inorganic nanomaterials were extensively used owing to the ease of synthesis and advantageous structural features [24–27]. For instance, layered double hydroxides (LDHs) – with general formula of $[M^{a+}_{1-x}M_x{}'^{b+}(OH)_2]^{y+}[A^{c-}_{y/c}]^{y+} \times zH_2O$; $y = a(1-x) + bx - 2$; where A^{c-} is an interlayer anion; M and M′ are metal cations – are well-known anion-intercalated 2D materials with significant anion exchange capacity [28–31]. In general, LDHs consist of octahedrally coordinated metal hydroxide layers ($[M^{a+}_{1-x}M'^{b+}_x(OH)_2]^{y+}$) including bivalent and trivalent cations and interlamellar, charge compensating, solvated anions ($[A^{c-}_{y/c}]^{y+} \times zH_2O$) [32–34]. LDH hosts possess great advantages in terms of their biocompatibility and their chemical and colloidal stability compared to *e.g.,* simple metal oxides [25,35].

For that reason, numerous studies focused on the key role of LDH hosts during antioxidant immobilization demonstrating the positive effects of LDHs on the flexibility and resistance of the antioxidant molecules [36–47]. Organic acids containing phenolic groups or polyphenols such as gallic acid [39,41], ferulic acid [40], ascorbic acid [37,47], BHPPA (3-(3,5-di-*tert*-butyl-4-hydroxy-phenyl)-propionic acid) [36], DBHP (3-(3,5-ditertbutyl-4-hydroxyphenyl) propionic acid) [43,44], Irganox 1425 [42], poly (butylene succinate) (PBS), 3-(4-Hydroxyphenyl)propionic acid (HPPA) [38], poly(lactic acid) [45,46] and 3-(4-hydroxyphenyl) propionate (HPP), L-tryptophan (TRP), and L-tyrosine (TYR) [47], were anchored on the outer surface of the LDHs or intercalated between their layers. Among others, it has already been shown that the LDH carriers enable antioxidants to operate as efficiently as their native (non-supported) forms [39,42]. Furthermore, by producing LDH/antioxidant/PP hybrid organic–inorganic composites, both the thermo-oxidative stability of poly(propylene) (PP) and the anti-migration ability of the antioxidants could be enhanced [42–44]. In almost all cases, the main goal was the elimination of the disadvantages of the native molecules that mainly originated from the poor water solubility. This challenge was addressed by utilizing the antioxidant protective effect of LDHs, which can be attributed to the strong chemical adhesion *via* adsorption/intercalation. Such structurally stable composites could be dispersed in significant amount. Moreover, LDH-involved composites showed prolonged release of the scavenger organics. However, the problem of difficult separation of the antioxidants used from the reaction mixtures still could not be addressed based on these immobilization methods.

TA/LDH composites containing also polymeric building blocks have already been prepared, but the studies published so far focused on the removal of pollutants instead of the antioxidant activity [48,49]. Besides, no comprehensive studies reporting on the effect of the synthetic methods on the molecular orientation within the composites have been disseminated so far. Consequently, there is a lack of information about the structure–activity relationship of molecular antioxidants once confined in composites. Note that neither LDH-supported nor any other heterogenized antioxidant systems have been studied comprehensively in terms of their recyclability and durability in radical scavenging reactions, albeit these are critical parameters in most of the applications.

The above-mentioned caveats and challenges motivated our research to control preparation methods of LDH-based antioxidant composites with special focus on the molecular orientation as well as local position of TA and glutathione (GSH). This study also aims to explore the possible changes in the activity of the supported molecular antioxidants due to structural orientations using several experimental techniques.

2. Experimental

2.1. Materials

Magnesium nitrate hexahydrate ($Mg(NO_3)_2{\cdot}6H_2O$), aluminium nitrate nonahydrate ($Al(NO_3)_3{\cdot}9H_2O$), NaOH solution, tannic acid (TA) and glutathione (GSH) were purchased from VWR International. These chemicals were analytical grade.

2.2. Synthesis of layered double hydroxides (LDHs)

The coprecipitation method was used to synthetize single-phase LDH particles of 2:1 magnesium(II)-to-aluminium(III) ratio. A mixed salt solution, containing $Mg(NO_3)_2 \times 6\ H_2O$ of 0.2 M (extra pure, VWR) and $Al(NO_3)_3 \times 9\ H_2O$ (ACS grade, VWR) of 0.1 M concentration was vigorously stirred under N_2 atmosphere. The pH was set to 10 by adding the appropriate amount of 4 M NaOH solution (ACS grade, VWR). After a 30-minute-long stirring, the slurry was centrifuged and washed with deionized water. The obtained solid was then redispersed and transferred into an autoclave followed by a heat-treatment at 120 °C overnight. The final product was centrifuged (4200 rpm, 10 min), washed with deionized water three times and dried at 50 °C in an oven overnight. For the synthe-

sis, the water was purified by a Puranity TU 3 + UV/UF system equipped with a UV irradiation unit (VWR).

2.3. Synthesis of antioxidant loaded LDHs

To produce antioxidant-LDH composites, two methods, namely adsorption and coprecipitation, were used. First, during the adsorption method, solid LDH powder of 0.5 g was redispersed in 10 mL of 0.1 M tannic acid (TA, high purity grade, VWR) solution. After one-day-long stirring under N_2 atmosphere, the sample was centrifuged (4200 rpm, 10 min), washed with deionized water three times and dried at 50 °C in an oven overnight. The final composite was denoted as LDH/TA/a. The same procedure was applied for glutathione (GSH, high purity grade, VWR) to obtain LDH/GSH/a.

Second, antioxidant loaded LDH particles were prepared by coprecipitation in the presence of TA or GSH. Accordingly, 0.01 mol $Mg(NO_3)_2 \times 6\,H_2O$, 0.005 mol $Al(NO_3)_3 \times 9\,H_2O$ and 0.005 mol GSH was dissolved in 50 mL deionized water. To set the pH to 10, appropriate amount of 4 M NaOH solution was added to the mixture. After one-day-long stirring under N_2 atmosphere, the sample was centrifuged (4200 rpm, 10 min), washed with deionized water three times and dried at 50 °C in an oven overnight. The final product was denoted as LDH/GSH/c. Almost the same procedure was applied for TA-loaded LDH (LDH/TA/c), except that up to a maximum TA amount of 0.0005 mol was used, as discussed later. The chemical structure of the natural antioxidants applied is shown in Fig. S1.

2.4. Structural and analytical characterization

Rigaku XRD-Miniflex II instrument operating with CuKα radiation (λ = 0.15418 nm) and 40 kV accelerating voltage at 30 mA was applied to measure X-ray diffractograms, which were recorded in the 2θ range of 3–80°, with a scan speed of 2°/minute. The characteristic reflections in the normalized diffractograms were identified on the basis of the information found in the JCPDS-ICDD (Joint Committee of Powder Diffraction Standards- International Centre for Diffraction Data) database.

Antioxidant content was detected with a Pfeiffer QMS 200 type mass spectrometer coupled with a Setaram LABSYS type thermogravimetric instrument. During the measurements, N_2 atmosphere and 10 °C/minute heating speed in the temperature range of 30–1000 °C was applied.

The FT-IR spectra were taken by a Nicolett™ Summit FT-IR spectrometer (Nicolet Instrument Company) with attenuated total reflection (ATR) detection mode using ZnSe-based ATR accessories. The spectra were collected in the range of 4000–400 cm^{-1} range, with 4 cm^{-1} resolution and 16 scans. No additional sample preparation procedure was applied before the measurements.

The Raman spectra were recorded with a Bruker Senterra II Raman microscope. Spectra of TA-containing LDH were collected by using a light source of 532 nm wavelength 12.5 mW laser power, while GSH loaded LDH was measured by applying a near-IR light source (785 nm) tuned at 100 mW laser power. Final data were obtained by averaging 32 spectra with an exposition time of 4 s. For the samples collected once the radical scavenging assays were terminated, the Raman spectra were recorded after centrifugation and drying of the solids. The instrumental settings were the same as described above.

For comparison, GSH and TA samples treated with NaOH were also prepared to correctly identify the vibrational bands of the guest molecules. Accordingly, 0.005 mol GSH or 0.0005 mol TA were dissolved in 50 mL deionized water. After adjusting the pH to 10 with 4 M NaOH/1 M HCl solutions, the samples were dried in an oven at 120 °C overnight. The IR and Raman spectra of the dried samples were recorded as previously described.

UV–Vis and NIR spectra were collected with a SHIMADZU UV-3600i Plus UV–vis-NIR spectrophotometer. The instrument is equipped with PMT, InGaAs, and PbS detectors. The spectra were measured in the 50000–6000 cm^{-1} range with 4 cm^{-1} resolution.

Morphology of the nanocomposites was studied by a Hitachi S-4700 scanning electron microscope (SEM) operating with 10 kV accelerating voltage. After sample immobilization on silicon wafer, to improve the conductivity of the sample surface, a thin gold layer was deposited on it.

2.5. Radical scavenging tests

A colour change-based spectrophotometric method was applied to determine radical scavenging activity of the native and immobilized antioxidants. The 2,2-diphenyl-1-picrylhydrazyl (DPPH) (≥95 %, VWR), a free radical with an absorption maximum at λ = 517 nm, was used as substrate in the assays [41]. The colour of the DPPH solution in methanol (AnalaR NORMAPUR Reag. Ph. Eur., ACS, VWR) is purple, which changes to yellow upon reaction with antioxidants. During the test, 3.5 mL of 24 mg/L DPPH solution was completed to 3.6 mL with antioxidant solutions, in which the concentration of the active substances was varied. The absorbance values were measured with a Genesys 10S UV–Vis spectrophotometer. By monitoring the change in absorbance at 517 nm, the remained percentage of DPPH was calculated:

$$\mathrm{DPPH}\,(\%) = \frac{A_1}{A_0} \tag{1}$$

where A_0 is the initial absorbance of the DPPH solution, while A_1 is the final absorbance value after the reaction between the radical and the antioxidant took place. For measurements with LDH composites, the corrected equation was used:

$$\mathrm{DPPH}\,(\%) = \frac{A_1\text{-}A_{sample}}{A_0} \tag{2}$$

where A_{sample} is the absorbance measured for the LDH composites dispersions without DPPH to detect any possible light scattering events by the particles.

By plotting DPPH (%) values as a function of the initial antioxidant concentration, the effective concentration (EC_{50}) was calculated. The EC_{50} is the antioxidant concentration required to decompose 50 % of free DPPH radicals in the test solution. The standard errors calculated from three independent measurements were within 5 %.

The recyclability assay for LDH/TA/a was performed on the basis of the DPPH test described above. More precisely, 4.2 mg LDH/TA/a was dispersed in 15 mL of free radical solution, in which the DPPH concentration was set to 23.3 mg/L (same as in the original protocol). After the appropriate reaction time, 1.5 mL solution was sampled and the absorbance was measured at 517 nm. Thereafter, to set the DPPH concentration to 23.3 mg/L again, the mixture was completed with the DPPH stock to 15 mL. These steps were repeated several times. For the better understanding, reduced DPPH (%) represented the amount of DPPH reacted during the individual steps of the reusability tests:

Reduced DPPH (%) = 100 % - DPPH (%) (3).

3. Results and discussion

3.1. Characterization of LDH/antioxidant composites

Fig. 1. shows the XRD patterns of the as-prepared host material. The peaks were attributed to the 00*l*, 01*l* and 11*l* series of Miller

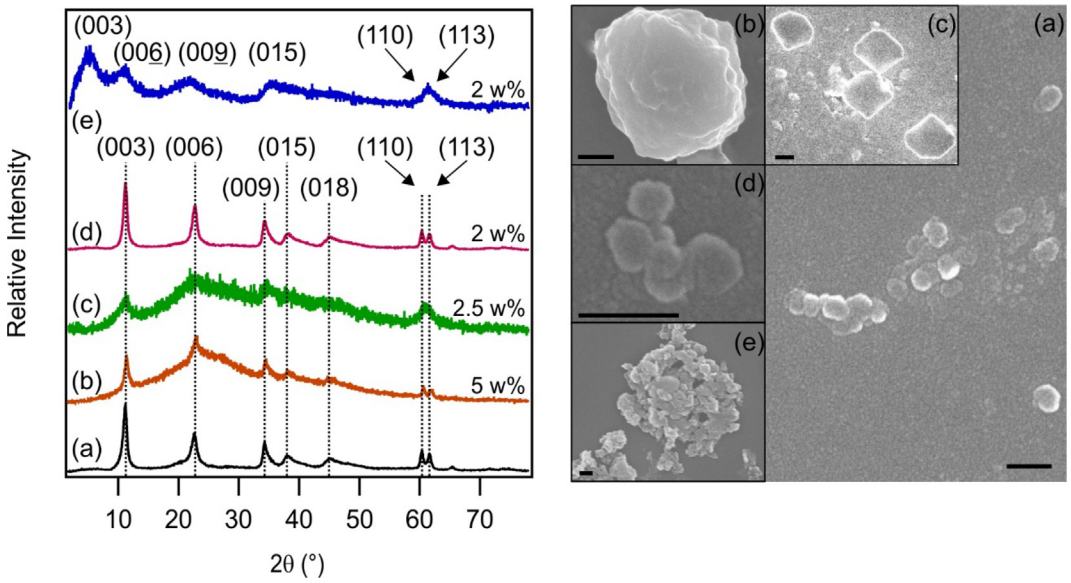

Fig. 1. XRD diffractograms and SEM micrographs of LDH (a), LDH/TA/a (b), LDH/TA/c (c), LDH/GSH/a (d), LDH/GSH/c (e). In the left, the Miller indices are indicated and the w% data refer to the antioxidant content in the composites. Scale bars represent 200 nm.

indices of a structure analogous to that of nitrate-containing LDHs (PDF# 35–0965) [50]. This result indicated that highly crystalline, single-phase lamellar LDH was obtained and that the interlamellar gallery was occupied by hydrated nitrate anions (d_{003} = 0.890 nm). No detectable variations in the location of the key reflections (003, 006, 009) were observed for LDH, LDH/TA/a, LDH/TA/c and LDH/GSH/a, which confirmed that no intercalation of the organic guests occurred. However, the shift in the position of 00*l* reflections of LDH/GSH/c is a proof for the expansion of the interlamellar gallery due to the intercalation of the GSH among the layers leading to strongly expanded d-spacing (d_{003} = 1.54 nm) compared to the one determined for the one-phase support LDH (d_{003} = 0.890 nm). The higher noise-to-signal ratio for LDH/TA/a and LDH/TA/c is the consequence of the lower crystallinity of the samples, but the characteristic LDH reflections also appeared for these materials indicating the formation of a long range-ordered LDH structure. Moreover, XRD measurements also revealed that maximum 0.01 M of TA concentration could be applied during coprecipitation to obtain LDH-like substances. Otherwise, at higher concentrations, TA was found to be a poison with negative effect on the crystal-growth of the LDH (Fig. S2.) leading to the absence of the lamellar structure.

The results of TG-MS measurements confirmed the presence of organic molecules in/on the LDH host in all cases. The total sorption values are expressed in terms of mass percentages of the organic molecules in relation to the total mass of the composites and are shown in Fig. 1 (left side). Specific adsorption of the guests led to variations in the organic contents and higher amount was determined in the TA-containing samples due to the higher molecular mass and number of functional groups of TA.

Morphological studies of the same materials were carried out with the SEM technique (Fig. 1). The average diameter for pure LDH was found to be (111 ± 17) nm. Similar to LDH, LDH/GSH/a and LDH/TA/c, the composites possessed plate-like, non-regular morphology with an average diameter of (115 ± 15) nm and (609 ± 227) nm, respectively. However, for LDH/GSH/c and LDH/TA/a, large aggregates were imaged and thus, no well-defined dimensions could be determined from the SEM micrographs. Because of the large-scale aggregation, these particles seemed to be more sphere-like compared to the above-mentioned composites.

FT-IR measurements were performed to further prove the presence of the organic compounds in the composites as well as to reveal the changes occurred in structure and conformation of TA and GSH upon immobilization on the LDH surface (Figs. 2 and 3). Only one strong band at 1356 cm^{-1} in the spectrum of the pure LDH host was identified, which corresponds to the stretching mode vibration of the NO_3^- groups [51]. This peak appears also in the spectra of all synthesized composites demonstrating the presence of interlamellar nitrate ions even if organic molecules were jointly intercalated. This is in line with literature data those reported partial ion exchanges for similar LDH systems [52].

For the accurate interpretation of the spectroscopy results for the composites, the IR spectra of both antioxidant molecules and their sodium hydroxide-treated counterparts were recorded and then resolved (Fig. 2b, c and 3b, c). The spectrum of the pure TA shows intense bands at 1178, 1308, 1335, 1380, 1443, 1513, 1534, 1605 and 1700 cm^{-1} wavenumbers. The strong bands around 1700 cm^{-1} and 1178 cm^{-1} can be associated with the stretching mode vibrations of carbonyl (C═O) and C—H groups, respectively [53]. The bands located at 1308, 1335 and 1380 cm^{-1} are identified as bending mode vibrations of phenolic groups [53]. The absorption bands corresponding to the stretching mode vibrations of C═C bond in the aromatic ring is observed at 1605 cm^{-1}, 1534 cm^{-1} and 1513 cm^{-1}, while the broad band at 1443 cm^{-1} is attributed to the bending mode vibration of the surface hydroxyl groups [54,55]. On the contrary, no well-resolved IR bands can be seen in the spectrum of the alkaline-treated TA. Hence, this finding implies that TA structure was damaged by the alkaline treatment.

From the spectra of the composites (Fig. 2d and 2e), it was concluded that the type of synthesis methods affected the immobilization of TA both qualitatively and quantitatively, governed the position of TA on the surface, but preserved its structural integrity. Indeed, the IR bands of the composites could be interpreted with the spectrum of pure TA. Thus, it is obvious that TA is prevented from alkaline disintegration in the presence of LDH host even if the coprecipitation took place at high pH.

However, significant deviations in the band positions can be observed for different composites depending on the molecular orientation of TA on the LDH surface upon immobilization [56]. For LDH/TA/c, a significant shift can be detected in the band positions

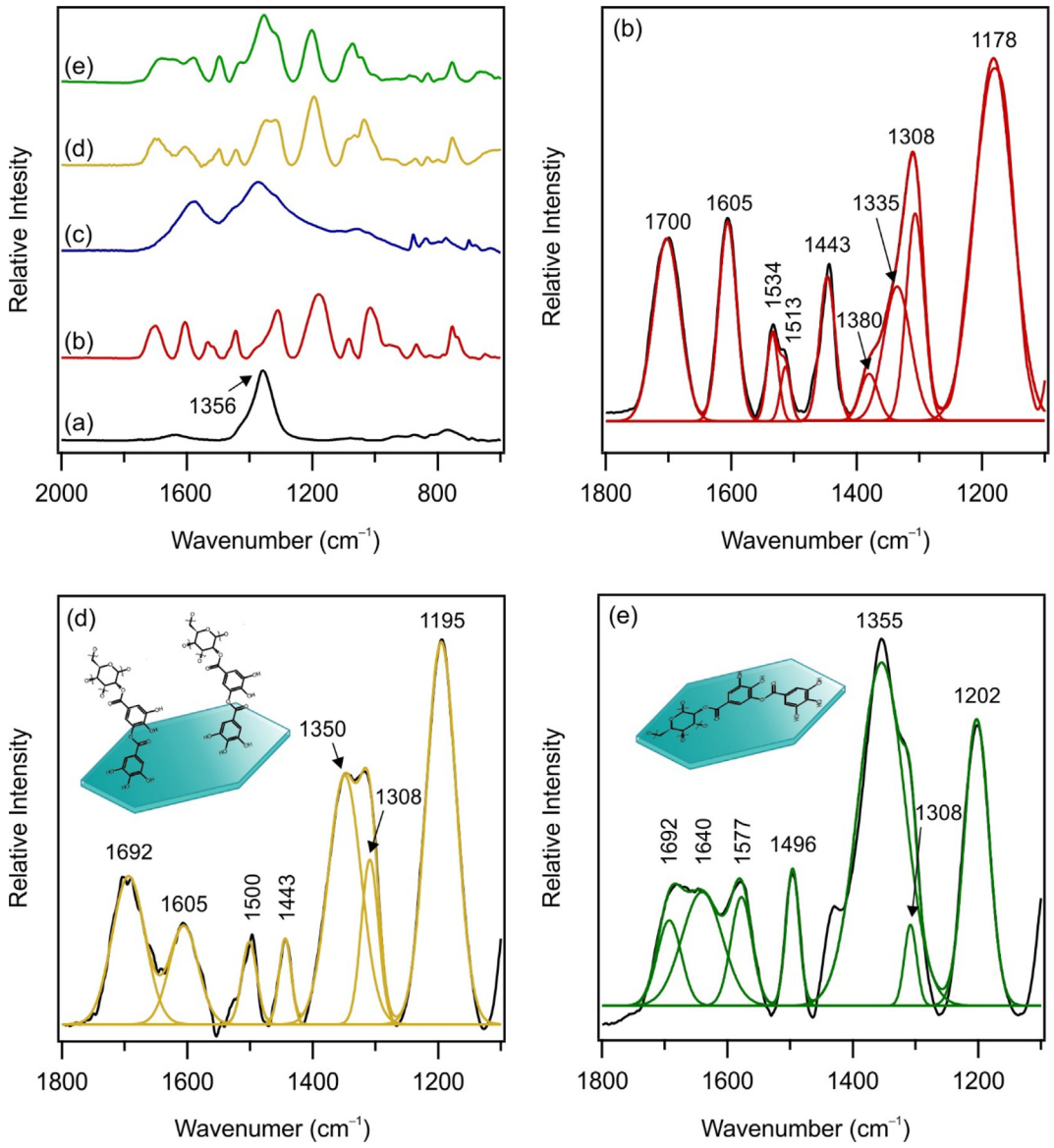

Fig. 2. FT-IR spectrum of LDH (a), TA (b), TA/NaOH (c), LDH/TA/a (d) and LDH/TA/c (e). The fitted curves for TA, LDH/TA/a and LDH/TA/c are shown separately too. The numbers indicate the wavenumber values, to which the peak positions were assigned. The schematic illustrations in (d) and (e) represent the different orientation of TA on the LDH surface.

of the hydroxyl groups (1443 cm^{-1} → 1496 cm^{-1}) and C=C bond (1513 cm^{-1} → 1640, 1577 cm^{-1}) of the aromatic rings. These bands, which were polarized in the direction of the molecular backbone, can be handled as markers for the orientation of TA on the surface of the host. These shifts imply that TA preferentially anchored parallel to the LDH surface in LDH/TA/c and thus, the vibrations of the ring and the hydroxyl groups are more hindered due to the interaction between the antioxidant molecule and the particle surface through electrostatic forces and hydrogen bonding. On the contrary, for LDH/TA/a, the positions and the relative intensities of the bands originating from ring vibrations closely resemble to those ones found in the literature [53] meaning that TA was immobilized perpendicularly on the LDH surface *via* the adsorption method. The detailed peak-assignment of TA loaded samples are collected in Table S1.

Based on the above results, the surface orientation of the adsorbed TA can be ruled by varying the synthesis method. This phenomenon is probably due to the differences in pH used. In the adsorption method, the pH was not adjusted, so most of the phenolic –OH groups are in the original (protonated) form, resulting in a low negative charge density of TA. Accordingly, the repulsive interactions between the hydrophilic surface and the hydrophobic aromatic rings of the molecules become dominant, so that TA is oriented in perpendicular to the surface. In contrast, the ionic/electrostatic interactions between the LDH surface and the TA molecules have largely evolved from the weak hydrophilic/hydrophobic interactions due to the fully deprotonated TA molecules generated at pH 10 set in the coprecipitation method [57]. As a direct result, the orientation of TA molecules is dominantly parallel to the LDH surface.

Raman spectroscopy measurements further confirmed our hypothesis (Fig. S3) [58]. The Raman band at 1612 cm^{-1}, assigned to the stretching mode vibration of C=C in the aromatic ring, deviates toward lower Raman shift values in the case of LDH/TA/c, while the characteristic bands are less altered in the spectrum of LDH/TA/a. Such a smaller change in the latter case is due mainly to the alteration in the total enthalpy caused by the adsorption process. This suggests that TA molecules interact by its aromatic

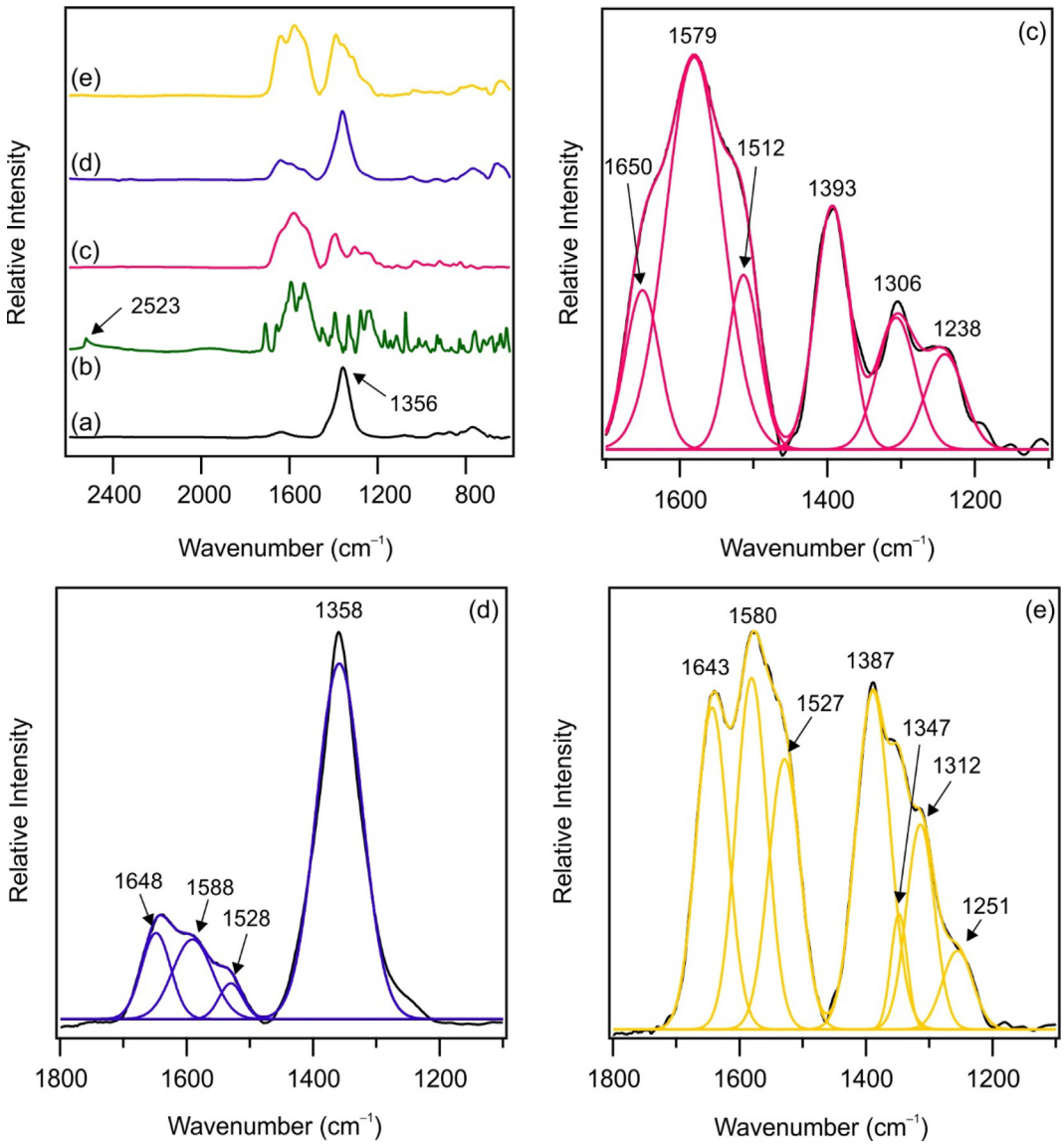

Fig. 3. FT-IR spectrum of LDH (a), GSH (b), GSH/NaOH (c), LDH/GSH/a (d) and LDH/GSH/c (e). The fitted curves for GSH/NaOH, LDH/GSH/a and LDH/GSH/c are shown separately. The inserted values indicate the characteristic peak positions in wavenumbers.

rings with the surface hydroxyl groups of the host upon parallel orientation in LDH/TA/c and that the characteristic vibrations are mainly hindered. Nevertheless, by anchoring TA perpendicularly on the LDH surface (LDH/TA/a), these vibrations of the aromatic rings of TA are free from any effects of the host, as mentioned above. The complete peak-assignment is shown in Table S2.

Furthermore, the type of synthetic route (either adsorption or coprecipitation) affected the GSH orientations in/on the LDH host, as revealed by the results of FT-IR and Raman spectroscopy measurements (Fig. 3 and Fig. S4, respectively). Alkaline treatment on the native GSH led to the formation of the GSH sodium salt and no structural disintegration could be observed at pH = 10. The IR spectra of the free and the adsorbed GSH (LDH/GSH/a) indicated that the guest molecules did not suffer any chemical (*e.g.*, deprotonation) or structural (*e.g.*, break in structure) transformations on the outer surface of LDH. The IR spectrum of the composite consisted of both the non-shifted characteristic vibration bands of the GSH (Amide I: 1658 cm^{-1} and Amide II: 1533 cm^{-1}) and the peak of the interlamellar nitrate ions (1358 cm^{-1}). In contrast, the sodium salt (*i.e.*, deprotonation occurred) of the GSH was immobilized during the coprecipitation process (LDH/GSH/c). Besides, the intense Amide III (1306 cm^{-1}) and Amide IV (1238 cm^{-1}) vibrations of the sodium salt of the GSH shifted significantly to the higher wavenumber region as a result of the immobilization, since identical bands were detected for the LDH/GSH/c and GSH/NaOH meaning that no peak could be assigned to the interlamellar nitrate. Considering these findings, one can note that the intercalation of GSH took place from the sodium salt during coprecipitation. This is in line with the results of the XRD measurements that the interlamellar space was completely occupied by GSH causing interlayer expansion without the appearance of the staging effect [59,60]. The full interpretation of the IR spectra are shown in Table S3. Note that the absence of the peak at 2523 cm^{-1}, that is assigned to the stretching mode vibration of the –SH group, for GSH loaded samples suggests the thiol deprotonation during the immobilization in both adsorption and coprecipitation approaches.

Raman measurements resulted in similar information on the immobilization scenarios at first glance (Fig. S4). However, further studies and analysis shed light on interesting features (Fig. S5) as

follows. On the one hand, the Raman spectra also confirmed the presence of the anionic form of GSH in in LDH/GSH/c. Moreover, the absence of the band around 2500 cm^{-1} in both LDH/GSH/a and LDH/GSH/c spectra is a clear evidence of the deprotonation of the thiol group during both synthetic processes [60]. On the other hand, in the spectral region of 700–200 cm^{-1}, there are some meaningful differences between the spectra of LDH/GSH/a and LDH/GSH/c (Fig. S5). Accordingly, an intense peak was observed at 510 cm^{-1} (denoted with black star) in the spectrum of LDH/GSH/c, which was assigned to the stretching mode vibration of the disulphide bond [61]. For LDH/GSH/a, this peak could not be identified, while the band related to the stretching mode vibration of the C—S moiety remained (labelled with black triangle) unchanged in comparison to LDH/GSH/c.

The above results raise the question that whether the redox activity of the thiolate group changed or not during the immobilization procedures or not. Upon using laser source of 532 nm instead of a source of 735 nm in the Raman study, the excitation of those thiolate groups, which presumably are in direct interaction with the host surface, occurs. The appearance of the peaks at 310 and 235 cm^{-1}, assigned to the stretching mode vibration of the thiolate–host bond, proved the presence of thiolate groups and thus, the joint presence of both GSH and GSSG (dimerized GSH through a disulphide bond) [62,63]. Furthermore, considering the dimensions of the expanded interlayer gallery presented before (Fig. 1), it is assumed that the deprotonated GSH fulfilled the interlamellar space, while the GSSG form occupied the outer surface of the host. The complete identification of the Raman shifts in the measured spectra is shown in Table S4.

Structural features of the composites were also explored by UV–VIS-NIR-DR spectroscopy (Fig. 4). The spectra were divided into three regions (200–500 nm: UV–VIS region; 1050–1350 nm and 1350–1700 nm: NIR region). The intense peak in the range of 1350–1700 nm is related to the first overtone of the fundamental hydroxyl stretching mode vibrations [64–66]. For antioxidant loaded samples, a systematic shift and broadening of this band

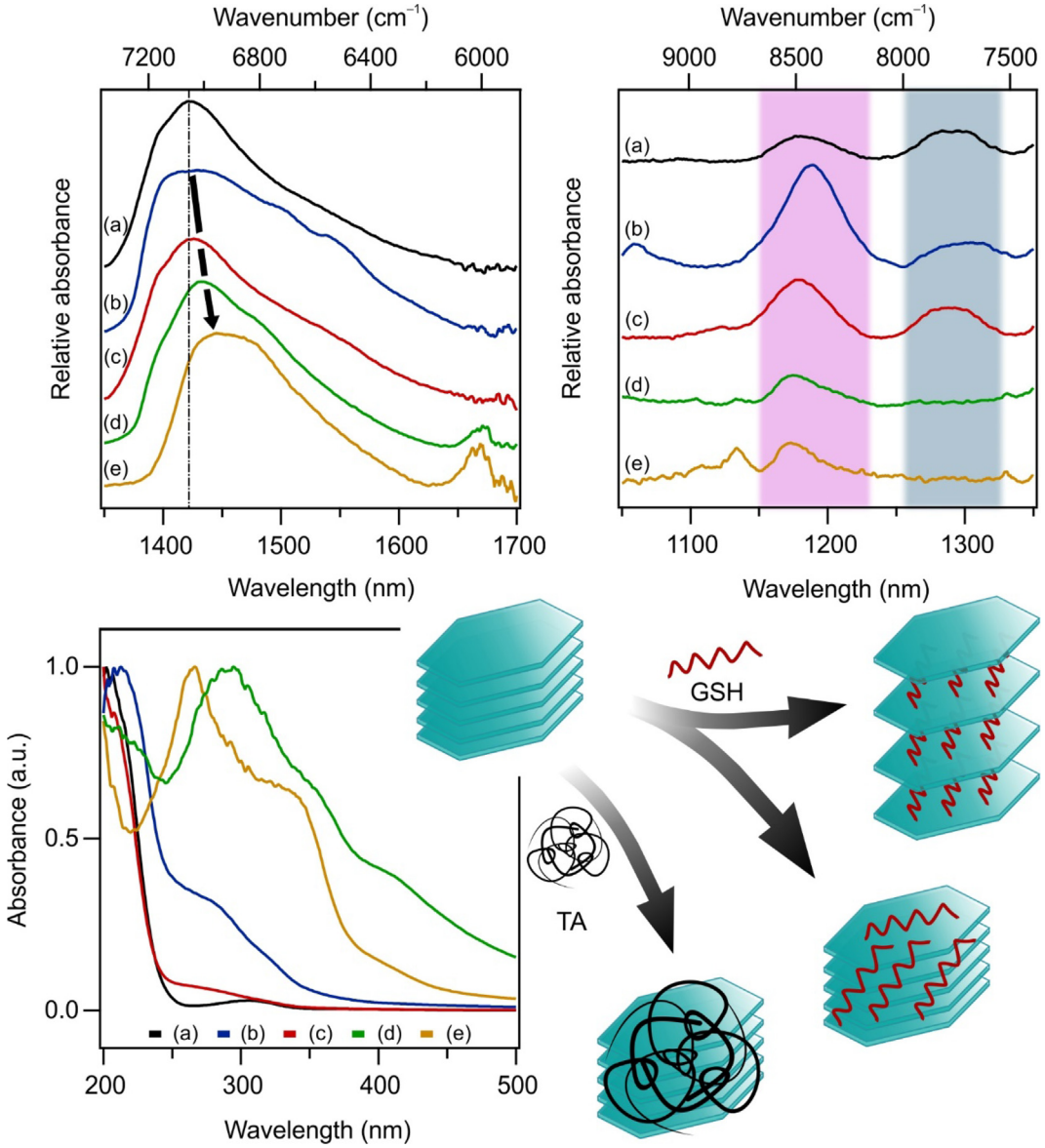

Fig. 4. UV–VIS-NIR spectra of LDH (a), LDH/GSH/c (b), LDH/GSH/a (c), LDH/TA/c (d) and LDH/TA/a (e). In the right-bottom corner, the schematic representation of the antioxidant immobilization is shown.

were detected, which can be associated with the appearance of the organic molecules in the composite structure causing significant changes in the polarity of the host surface [67]. The shift is more visible for LDH/TA/a and LDH/TA/c, which can be due to the pronounced hydrophobic character of TA. The interaction between the hydrophobic framework of TA and the surface OH groups of LDH may lead to larger shifts in the spectra. For LDH, two low intensity peaks were observed in the spectral range of 1050–1350 nm, similar to previously reported cases [68]. The peaks are related to the first overtone of the symmetrical stretching mode vibration of hydroxyl groups and combination bands of the "free water" [65]. The variations in this region are closely attributed to the decrease in the number of the surface adsorbed water molecules. Accordingly, by using adsorption method, the intensity of this group decreased significantly.

Remarkable changes in the spectra of the obtained materials were detected in the UV–VIS range (200–500 nm) as well. There is no considerable absorbance of the LDH host in this spectral region, while for antioxidant loaded LDHs, significant differences were observed, which deserves further discussion. Accordingly, for GSH-containing samples, an absorption band appeared around 270 nm, which belongs to the GSH molecules [69]. However, for LDH/GSH/c, an additional absorption maximum at 213 nm was also recorded, which is related to the presence of GSSG [70] in accordance with the results of the Raman spectroscopy measurements. Note that these maxima are shifted in comparison to the literature data [69,70]. The peaks at 267 nm and at 294 nm for LDH/TA/a and LDH/TA/c, respectively, closely resemble the data found in the literature (278 nm), however, notable shifts can be observed [71]. Overall, the substantial changes in the UV–VIS-NIR spectra of the composites should be interpreted as a proof for the formation of chemical adhesion, which was found as the main interaction during adsorption. For LDH/GSH/c, the molecules in the interlamellar region were attached by ionic interactions to the host during intercalation (Fig. 4). In fact, the actual molar ratio between the interlamellar GSH and the adsorbed GSSG molecules could not be determined. However, considering the significant variations in the UV spectral range, it could be assumed that the adsorbed specimens coexisted in significant amounts compared to the interlamellar ones.

3.2. Structure-activity relationship

To estimate the antioxidant activity of the composites, DPPH assays were performed. During the test reaction, a stable organic radical is being reduced by the antioxidant molecules, which causes colour change in the solution. The results obtained for the native and immobilized antioxidants are shown in Fig. 5.

The antioxidant activity of the TA remained high, even somewhat higher than for native TA, upon immobilization by adsorption (LDH/TA/a). On the contrary, LDH/TA/c was found to be almost inactive in the test reactions. These results shed light on the correlation between the antioxidant ability and the orientation of TA in the composites. By anchoring perpendicularly to the LDH sheets (LDH/TA/a), the TA molecules are active and hence, the accessibility of the phenolic groups for the radicals was improved giving rise to enhancement in the antioxidant activity of TA. Nevertheless, the use of coprecipitation approach confined the majority of the phenolic groups close to the interface such that the TA molecules adsorbed in a plane parallel to the surface leading to very limited or even negligible accessibility of the active groups to the DPPH substrate. Therefore, LDH/TA/c did not show significant antioxidant effect. The scavenging activity of TA as well as LDH/TA/a was the same within the experimental error up to one month storage time.

For the GSH-containing systems, the DPPH decomposing activity did not change significantly after immobilization irrespective to the preparation procedures used. Accordingly, the activities of both LDH/GSH/a and LDH/GSH/c were similar to the native molecule (Fig. 5). These results are in good agreement with novel findings, in which various synthetic pathways were reported to prepare antioxidant–LDH nanohybrids without losing the antioxidant activity of the intercalant [42–44]. Long-term activity measurements revealed that the scavenging ability of the native GSH increased by time, *i.e.*, the EC_{50} value decreased significantly after 1 month. However, it is known that GSH undergoes self-

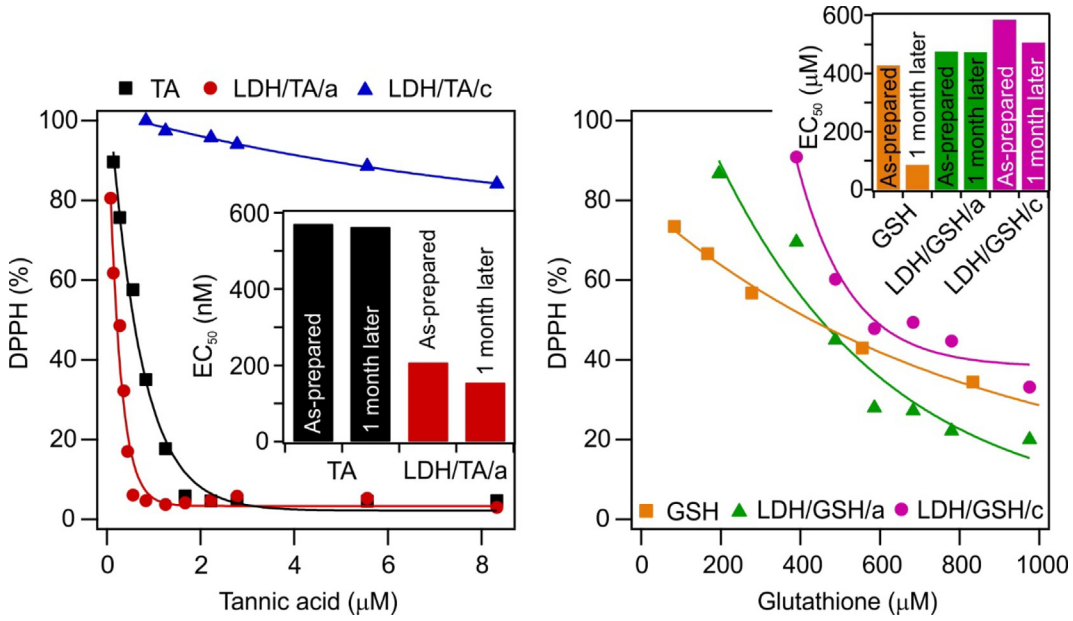

Fig. 5. Remaining DPPH as a function of the antioxidant concentration for the native and immobilized TA (left) and GSH (right). The bar graphs show the EC_{50} values determined for the fresh (as-prepared) and 1 month old samples.

decomposition in this timeframe [72]. Being smaller and more hydrophobic molecules with more accessible thiol groups, the decomposition products of native GSH may have higher antioxidant activity. However, their quantities and relative ratios to each other are difficult to control due to their enhanced reactivity in comparison to the native GSH [73]. Thus, their application in industrial processes or by natural organisms are severely hindered. Nevertheless, the EC_{50} value determined after 1 month belongs to the products of decomposition and such an activity cannot be directly compared to that determined for the fresh samples. In case of LDH/GSH/a and LDH/GSH/c the antioxidant efficiency remained about the same for the period investigated meaning that the structure of GSH was stabilized upon immobilization and that GSH decompose neither on (LDH/GSH/a) nor in (LDH/GSH/c) the LDH support. This result unambiguously sheds light on the stabilizing role of the LDH host. Similar role was not published previously for LDHs.

After applying the composites in the DPPH assays, their structure was investigated by IR (Fig. S6) and Raman (Fig. S7) spectroscopy to identify possible structural changes occurred during the test reactions. About the same IR and Raman spectra were recorded before and after the assays indicating that these composites kept their structural integrity upon reaction with DPPH radicals.

Based on these results, reusability/recyclability tests were carried out for the most active composite, namely LDH/TA/a, by determining the reduced DPPH (%) values (equation 3) defined in the experimental part. At the end of a reaction cycle, a portion of the sample was taken for the analyses. However, in each cycle, both the total volume of the reaction mixture and the concentration of the immobilized antioxidants as well as the DPPH content were kept at a constant value. The results are shown in Fig. 6. The antioxidant activity of LDH/TA/a remained approximately the same at a reduced DPPH (%) value of 80 % during 15 runs, however, the antioxidant activity decreased gradually thereafter reaching reduced DPPH (%) of 20 % after the 25th cycle. These results indicate excellent recyclability of the antioxidant materials, which is a crucial parameter in further applications. The developed synthetic methodologies offer a feasible route to create reusable antioxidants of ability to fix, in particular, industrially relevant problems related to elevated ROS level.

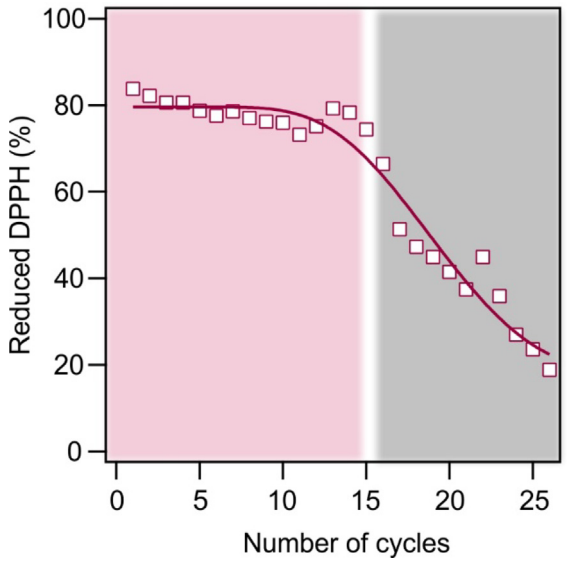

Fig. 6. Reusability of LDH/TA/a expressed in reduced DPPH data as a function of the reaction cycles.

4. Conclusions

Molecular antioxidants, tannic acid (TA) and glutathione (GSH), were successfully immobilized in/on layered double hydroxides (LDHs). By altering the preparation method, significant differences were observed between the molecular orientation of the anchored antioxidants in the composites. TA adopted perpendicular or parallel orientation to the LDH sheets once adsorption or coprecipitation, respectively, was applied during synthesis. GSH forms dimers during immobilization, while deprotonation took place upon adsorption of single molecules. These forms exist jointly in the composites. Radical scavenging tests indicated clear structure–activity relation, which was clarified in various spectroscopy measurements. By anchoring TA on a parallel position to the surface via the coprecipitation method, negligible activity was determined. On the contrary, in a perpendicular interfacial position achieved via the adsorption method, the TA demonstrated higher activity than the native antioxidant in solution. Coprecipitation led to GSH intercalation among the layers of the LDH host, while physical adsorption method to the surface anchoring of GSH. However, the radical scavenging activity of the GSH was independent from the type of immobilization methods. In addition, the heterogenization of the antioxidants gave rise to two unexpected results. First, the GSH containing composites possessed notable durability, since no changes were detected in the GSH activity after a month, while the structure was maintained in contrast to homogeneous GSH solutions. Hence, an important drawback of the long-term use of this native antioxidant was solved. Second, LDH/TA/a could be recycled several times, while keeping its antioxidant ability without significant loss in its function. This result makes the composites a promising antioxidant agent to be applied even in industrial processes, wherever elevated ROS concentration is a problem to be solved.

Author Contributions

The manuscript was written through contributions of all authors. All authors have given approval to the final version of the manuscript.

CRediT authorship contribution statement

Adél Szerlauth: Conceptualization, Methodology, Investigation, Formal analysis, Writing – original draft. **Zsuzsanna D. Kónya:** Investigation. **Gréta Papp:** Investigation. **Zoltán Kónya:** Validation, Resources. **Ákos Kukovecz:** Validation, Resources. **Márton Szabados:** Investigation. **Gábor Varga:** Conceptualization, Supervision, Formal analysis, Writing – original draft, Writing – review & editing. **István Szilágyi:** Conceptualization, Supervision, Writing – original draft, Writing – review & editing.

Data availability

Data will be made available on request.

Declaration of Competing Interest

The authors declare that they have no known competing financial interests or personal relationships that could have appeared to influence the work reported in this paper.

Acknowledgements

The research was financially supported by the ELRN/HAS through the Lendület program and by project no. TKP2021-NVA-

19, which has been implemented with the support provided by the Ministry of Innovation and Technology of Hungary from the National Research, Development and Innovation Fund, financed under the TKP2021-NVA funding scheme. This work was also supported by the University of Szeged Open Access Fund (Grant number: 5964).

Appendix A. Supplementary material

Supplementary data to this article can be found online at https://doi.org/10.1016/j.jcis.2022.11.056.

References

[1] J.M. McCord, I. Fridovich, Superoxide Dismutase, J. Biol. Chem. 244 (1969) 6049–6055, https://doi.org/10.1016/S0021-9258(18)63504-5.
[2] Y. Zeng, G. Liu, T. Lv, X. He, Y. Wei, R. Pan, L. Yang, L. Tao, Antioxidant Polymers via the Ugi Reaction for In Vivo Protection of UV-Induced Oxidative Stress, Chem. Mater. 34 (2022) 2645–2654, https://doi.org/10.1021/acs.chemmater.1c03897.
[3] S. Kumar, J. Yan, J. Poon, V.P. Singh, X. Lu, M. Karlsson Ott, L. Engman, S. Kumar, Multifunctional Antioxidants: Regenerable Radical-Trapping and Hydroperoxide-Decomposing Ebselenols, Angew. Chem. 128 (2016) 3793–3797, https://doi.org/10.1002/ange.201510947.
[4] W.C. Geng, D. Zhang, C. Gong, Z. Li, K.M. Barraza, J.L. Beauchamp, D.S. Guo, X. Zhang, Host-Guest Complexation of Amphiphilic Molecules at the Air-Water Interface Prevents Oxidation by Hydroxyl Radicals and Singlet Oxygen, Angew. Chem. Int. Ed. 59 (2020) 12684–12688, https://doi.org/10.1002/anie.202001355.
[5] A. Bafana, S. Dutt, S. Kumar, P.S. Ahuja, Superoxide dismutase: An industrial perspective, Crit. Rev. Biotechnol. 31 (2011) 65–76, https://doi.org/10.3109/07388551.2010.490937.
[6] A. Rigoussen, P. Verge, J.M. Raquez, P. Dubois, Natural Phenolic Antioxidants As a Source of Biocompatibilizers for Immiscible Polymer Blends, ACS Sustain. Chem. Eng. 6 (2018) 13349–13357, https://doi.org/10.1021/acssuschemeng.8b02999.
[7] J. Brito, H. Hlushko, A. Abbott, A. Aliakseyeu, R. Hlushko, S.A. Sukhishvili, Integrating Antioxidant Functionality into Polymer Materials: Fundamentals, Strategies, and Applications, ACS Appl. Mater. Interfaces. 13 (2021) 41372–41395, https://doi.org/10.1021/acsami.1c08061.
[8] Y. Dai, T. Li, Z. Zhang, Y. Tan, S. Pan, L. Zhang, H. Xu, Oxidative Polymerization in Living Cells, J. Am. Chem. Soc. 143 (2021) 10709–10717, https://doi.org/10.1021/jacs.1c04821.
[9] J. Bouayed, T. Bohn, Exogenous antioxidants - Double-edged swords in cellular redox state: Health beneficial effects at physiologic doses versus deleterious effects at high doses, Oxid. Med. Cell. Longev. 3 (2010) 228–237, https://doi.org/10.4161/oxim.3.4.12858.
[10] H. Sies, D.P. Jones, Reactive oxygen species (ROS) as pleiotropic physiological signalling agents, Nat. Rev. Mol. Cell Biol. 21 (2020) 363–383, https://doi.org/10.1038/s41580-020-0230-3.
[11] C.C. Winterbourn, Reconciling the chemistry and biology of reactive oxygen species, Nat. Chem. Biol. 4 (2008) 278–286, https://doi.org/10.1038/nchembio.85.
[12] B. Kirschweng, D. Tátraaljai, E. Földes, B. Pukánszky, Natural antioxidants as stabilizers for polymers, Polym. Degrad. Stab. 145 (2017) 25–40, https://doi.org/10.1016/j.polymdegradstab.2017.07.012.
[13] I. Kriston, Á. Orbán-Mester, G. Nagy, P. Staniek, E. Földes, B. Pukánszky, Melt stabilisation of Phillips type polyethylene, Part I: The role of phenolic and phosphorous antioxidants, Polym. Degrad. Stab. 94 (2009) 719–729, https://doi.org/10.1016/j.polymdegradstab.2008.12.011.
[14] D. Brocca, E. Arvin, H. Mosbæk, Identification of organic compounds migrating from polyethylene pipelines into drinking water, Water Res. 36 (2002) 3675–3680, https://doi.org/10.1016/S0043-1354(02)00084-2.
[15] V.M. Gol'dberg, G.E. Zaikov, Kinetics of mechanical degradation in melts under model conditions and during processing of polymers-A review, Polym. Degrad. Stab. 19 (3) (1987) 221–250.
[16] K. Thangaraj, J. Li, H. Mei, S. Hu, R. Han, Z. Zhao, X. Chen, X. Li, D. Kamatchi Reddiar, Mycorrhizal Colonization Enhanced Sorghum bicolor Tolerance under Soil Water Deficit Conditions by Coordination of Proline and Reduced Glutathione (GSH), J. Agric. Food Chem. 70 (2022) 4243–4255, https://doi.org/10.1021/acs.jafc.1c07184.
[17] M. Chen, S. Zhao, J. Zhu, E. Feng, F. Lv, W. Chen, S. Lv, Y. Wu, X. Peng, F. Song, Open-Source and Reduced-Expenditure Nanosystem with ROS Self-Amplification and Glutathione Depletion for Simultaneous Augmented Chemodynamic/Photodynamic Therapy, ACS Appl. Mater. Interfaces. 14 (2022) 20682–20692, https://doi.org/10.1021/acsami.2c01782.
[18] A.I. Benítez-Mateos, D. Roura Padrosa, F. Paradisi, Multistep enzyme cascades as a route towards green and sustainable pharmaceutical syntheses, Nat. Chem. 14 (2022) 489–499, https://doi.org/10.1038/s41557-022-00931-2.
[19] R. Kubota, S. Asayama, H. Kawakami, Catalytic antioxidants for therapeutic medicine, J. Mater. Chem. B. 7 (2019) 3165–3191, https://doi.org/10.1039/c8tb03365j.
[20] C. Martinelli, C. Pucci, M. Battaglini, A. Marino, G. Ciofani, Antioxidants and Nanotechnology: Promises and Limits of Potentially Disruptive Approaches in the Treatment of Central Nervous System Diseases, Adv. Healthc. Mater. 9 (2020) 1–28, https://doi.org/10.1002/adhm.201901589.
[21] A.D. Castilloux, M. Houde, A. Gendron, A. De Silva, Y.D. Soubaneh, Z. Lu, Distribution and Fate of Ultraviolet Absorbents and Industrial Antioxidants in the St. Lawrence River, Quebec, Canada, Environ. Sci. Technol. 56 (8) (2022) 5009–5019.
[22] K. Saravana Mani, W. Kaminsky, S.P. Rajendran, A facile atom economic one pot multicomponent synthesis of bioactive spiro-indenoquinoxaline pyrrolizines as potent antioxidants and anti-cancer agents, New J. Chem. 42 (2018) 301–310, https://doi.org/10.1039/c7nj02993d.
[23] H.J. Forman, H. Zhang, Targeting oxidative stress in disease: promise and limitations of antioxidant therapy, Nat. Rev. Drug Discov. 20 (2021) 689–709, https://doi.org/10.1038/s41573-021-00233-1.
[24] S.P. Lonkar, B. Kutlu, A. Leuteritz, G. Heinrich, Nanohybrids of phenolic antioxidant intercalated into MgAl-layered double hydroxide clay, Appl. Clay Sci. 71 (2013) 8–14, https://doi.org/10.1016/j.clay.2012.10.009.
[25] A. Szerlauth, S. Muráth, I. Szilagyi, Layered double hydroxide-based antioxidant dispersions with high colloidal and functional stability, Soft Matter. 16 (2020) 10518–10527, https://doi.org/10.1039/d0sm01531h.
[26] L. Valgimigli, A. Baschieri, R. Amorati, Antioxidant activity of nanomaterials, J. Mater. Chem. B. 6 (2018) 2036–2051, https://doi.org/10.1039/c8tb00107c.
[27] S. Farouk, S.M. Al-Amri, Ameliorative roles of melatonin and/or zeolite on chromium-induced leaf senescence in marjoram plants by activating antioxidant defense, osmolyte accumulation, and ultrastructural modification, Ind. Crops Prod. 142 (2019), https://doi.org/10.1016/j.indcrop.2019.111823 111823.
[28] S. Muráth, T. Varga, Á. Kukovecz, Z. Kónya, P. Sipos, I. Pálinkó, G. Varga, Morphological aspects determine the catalytic activity of porous hydrocalumites: the role of the sacrificial templates, Mater. Today Chem. 23 (2022) 100682.
[29] M. Pavlovic, P. Rouster, T. Oncsik, I. Szilagyi, Tuning Colloidal Stability of Layered Double Hydroxides: From Monovalent Ions to Polyelectrolytes, ChemPlusChem. 82 (2017) 121–131, https://doi.org/10.1002/cplu.201600295.
[30] G. Varga, Z. Somosi, Z. Kónya, Á. Kukovecz, I. Pálinkó, I. Szilagyi, A colloid chemistry route for the preparation of hierarchically ordered mesoporous layered double hydroxides using surfactants as sacrificial templates, J. Colloid Interface Sci. 581 (2021) 928–938, https://doi.org/10.1016/j.jcis.2020.08.118.
[31] V.R.R. Cunha, P.A.D. Petersen, R.B. Souza, Ana Maria C.R.P.F. Martins, F. Leroux, C. Taviot-Gueho, H.M. Petrilli, I.H.J. Koh, V.R.L. Constantino, Phytochemical species intercalated into layered double hydroxides: Structural investigation and biocompatibility assays, New J. Chem. 44 (2020) 10011–10021, https://doi.org/10.1039/d0nj00238k.
[32] M. Laipan, J. Yu, R. Zhu, J. Zhu, A.T. Smith, H. He, D. O'Hare, L. Sun, Functionalized layered double hydroxides for innovative applications, Mater. Horizons. 7 (2020) 715–745, https://doi.org/10.1039/c9mh01494b.
[33] C. Taviot-Guého, V. Prévot, C. Forano, G. Renaudin, C. Mousty, F. Leroux, Tailoring Hybrid Layered Double Hydroxides for the Development of Innovative Applications, Adv. Funct. Mater. 28 (2018) 1703868, https://doi.org/10.1002/adfm.201703868.
[34] J. Liu, L. Sun, L. Li, R. Zhang, Z.P. Xu, Synergistic Cancer Photochemotherapy via Layered Double Hydroxide-Based Trimodal Nanomedicine at Very Low Therapeutic Doses, ACS Appl. Mater. Interfaces. 13 (2021) 7115–7126, https://doi.org/10.1021/acsami.0c23143.
[35] Y. Liu, Y. Wu, R. Zhang, J. Lam, J.C. Ng, Z.P. Xu, L. Li, H.T. Ta, Investigating the Use of Layered Double Hydroxide Nanoparticles as Carriers of Metal Oxides for Theranostics of ROS-Related Diseases, ACS Appl. Bio Mater. 2 (2019) 5930–5940, https://doi.org/10.1021/acsabm.9b00852.
[36] Y. Feng, Y. Jiang, Q. Huang, S. Chen, F. Zhang, P. Tang, D. Li, High antioxidative performance of layered double hydroxides/polypropylene composite with intercalation of low-molecular-weight phenolic antioxidant, Ind. Eng. Chem. Res. 53 (2014) 2287–2292, https://doi.org/10.1021/ie403643v.
[37] X. Gao, L. Lei, D. O'Hare, J. Xie, P. Gao, T. Chang, Intercalation and controlled release properties of vitamin C intercalated layered double hydroxide, J. Solid State Chem. 203 (2013) 174–180, https://doi.org/10.1016/j.jssc.2013.04.028.
[38] G. Totaro, L. Sisti, A. Celli, H. Askanian, M. Hennous, V. Verney, F. Leroux, Chain extender effect of 3-(4-hydroxyphenyl)propionic acid/layered double hydroxide in PBS bionanocomposites, Eur. Polym. J. 94 (2017) 20–32, https://doi.org/10.1016/j.eurpolymj.2017.06.031.
[39] K.M. Ansy, J.H. Lee, H. Piao, G. Choi, J.H. Choy, Stabilization of antioxidant gallate in layered double hydroxide by exfoliation and reassembling reaction, Solid State Sci. 80 (2018) 65–71, https://doi.org/10.1016/j.solidstatesciences.2018.04.001.
[40] E. Lima, J. Flores, A.S. Cruz, G. Leyva-Gómez, E. Krötzsch, Controlled release of ferulic acid from a hybrid hydrotalcite and its application as an antioxidant for human fibroblasts, Microporous Mesoporous Mater. 181 (2013) 1–7, https://doi.org/10.1016/j.micromeso.2013.07.014.
[41] X. Kong, L. Jin, M. Wei, X. Duan, Antioxidant drugs intercalated into layered double hydroxide: Structure and in vitro release, Appl. Clay Sci. 49 (2010) 324–329, https://doi.org/10.1016/j.clay.2010.06.017.
[42] Q. Zhang, Q. Jiao, F. Leroux, P. Tang, D. Li, Y. Feng, Antioxidant intercalated hydrocalumite as multifunction nanofiller for Poly(propylene): Synthesis, thermal stability, light stability, and anti-migration property, Polym. Degrad. Stab. 140 (2017) 9–16, https://doi.org/10.1016/j.polymdegradstab.2017.04.012.

[43] Q. Zhang, Q. Jiao, F. Leroux, P. Tang, D. Li, Y. Feng, Antioxidant intercalated Zn-containing layered double hydroxides: preparation, performance and migration properties, New J. Chem. 41 (2017) 2364–2371, https://doi.org/10.1039/C6NJ03544B.
[44] Q. Zhang, Y. Guo, A.A. Marek, V. Verney, F. Leroux, P. Tang, D. Li, Y. Feng, Design, fabrication and anti-aging behavior of a multifunctional inorganic-organic hybrid stabilizer derived from co-intercalated layered double hydroxides for polypropylene, Inorg. Chem. Front. 6 (2019) 2539–2549, https://doi.org/10.1039/c9qi00601j.
[45] S. Coiai, S. Javarone, F. Cicogna, W. Oberhauser, M. Onor, A. Pucci, P. Minei, G. Iasilli, E. Passaglia, Fluorescent LDPE and PLA nanocomposites containing fluorescein-modified layered double hydroxides and their ON/OFF responsive behavior towards humidity, Eur. Polym. J. 99 (2018) 189–201, https://doi.org/10.1016/j.eurpolymj.2017.12.021.
[46] N. Delpouve, A. Saiter-Fourcin, S. Coiai, F. Cicogna, R. Spiniello, W. Oberhauser, S. Legnaioli, R. Ishak, E. Passaglia, Effects of organo-LDH dispersion on thermal stability, crystallinity and mechanical features of PLA, Polymer (Guildf). 208 (2020), https://doi.org/10.1016/j.polymer.2020.122952 122952.
[47] A.A. Marek, V. Verney, G. Totaro, L. Sisti, A. Celli, N. Bozzi Cionci, D. Di Gioia, L. Massacrier, F. Leroux, Organo-modified LDH fillers endowing multi-functionality to bio-based poly(butylene succinate): An extended study from the laboratory to possible market, Appl. Clay Sci. 188 (2020), https://doi.org/10.1016/j.clay.2020.105502 105502.
[48] Q. Huang, J. Zhao, M. Liu, J. Chen, X. Zhu, T. Wu, J. Tian, Y. Wen, X. Zhang, Y. Wei, Preparation of polyethylene polyamine@tannic acid encapsulated MgAl-layered double hydroxide for the efficient removal of copper (II) ions from aqueous solution, J. Taiwan Inst. Chem. Eng. 82 (2018) 92–101, https://doi.org/10.1016/j.jtice.2017.10.019.
[49] S. Mallakpour, Z. Radfar, M. Feiz, Optimization of chitosan/tannic acid@ ZnFe layered double hydroxide bionanocomposite film for removal of reactive blue 4 using a response surface methodology, Int. J. Biol. Macromol. 209 (2022) 747–762, https://doi.org/10.1016/j.ijbiomac.2022.04.020.
[50] D. Zhang, X.Y. Liu, H.T. Zhao, L. Yang, T. Lü, M.Q. Jin, Application of hydrotalcite in soil immobilization of iodate (IO_3^-), RSC Adv. 8 (2018) 21084–21091, https://doi.org/10.1039/c8ra04013c.
[51] G. Varga, V. Kozma, V.J. Kolcsár, Á. Kukovecz, Z. Kónya, P. Sipos, I. Pálinkó, G. Szőllősi, β-Isocupreidinate-CaAl-layered double hydroxide composites–heterogenized catalysts for asymmetric Michael addition, Mol. Catal. 482 (2020) 110675.
[52] V. Rives, M.A. Ulibarri, Layered double hydroxides (LDH) intercalated with metal coordination compounds and oxometalates, Coord. Chem. Rev. 181 (1999) 61–120, https://doi.org/10.1016/S0010-8545(98)00216-1.
[53] X. Liang, K. Cao, W. Li, X. Li, D.J. McClements, K. Hu, Tannic acid-fortified zein-pectin nanoparticles: Stability, properties, antioxidant activity, and in vitro digestion, Food Res. Int. 145 (2021), https://doi.org/10.1016/j.foodres.2021.110425 110425.
[54] S. Aswathy Aromal, D. Philip, Facile one-pot synthesis of gold nanoparticles using tannic acid and its application in catalysis,, Phys. E Low-Dimensional Syst. Nanostructures. 44 (2012) 1692–1696, https://doi.org/10.1016/j.physe.2012.04.022.
[55] S.L. Cumberland, G.F. Strouse, Analysis of the nature of oxyanion adsorption on gold nanomaterial surfaces, Langmuir. 18 (2002) 269–276, https://doi.org/10.1021/la011278n.
[56] S.D. Evans, E. Urankar, A. Ulman, N. Ferris, Self-assembled monolayers of alkanethiols containing a polar aromatic group: effects of the dipole position on molecular packing, orientation, and surface wetting properties, J. Am. Chem. Soc. 113 (1991) 4121–4131, https://doi.org/10.1021/ja00011a010.
[57] G. Ghigo, S. Berto, M. Minella, D. Vione, E. Alladio, V.M. Nurchi, J. Lachowicz, P. G. Daniele, New insights into the protogenic and spectroscopic properties of commercial tannic acid: The role of gallic acid impurities, New J. Chem. 42 (2018) 7703–7712, https://doi.org/10.1039/c7nj04903j.
[58] S. Mazurek, I. Fecka, M. Węglińska, R. Szostak, Quantification of active ingredients in Potentilla tormentilla by Raman and infrared spectroscopy, Talanta. 189 (2018) 308–314, https://doi.org/10.1016/j.talanta.2018.07.012.
[59] M. Picquart, L. Grajcar, M.H. Baron, Z. Abedinzadeh, Vibrational spectroscopic study of glutathione complexation in aqueous solutions, Biospectroscopy. 5 (1999) 328–337, https://doi.org/10.1002/(SICI)1520-6343(1999)5:6<328::AID-BSPY2>3.0.CO;2-J.
[60] S. Catalini, B. Rossi, P. Foggi, C. Masciovecchio, F. Bruni, Aqueous solvation of glutathione probed by UV resonance Raman spectroscopy, J. Mol. Liq. 283 (2019) 537–547, https://doi.org/10.1016/j.molliq.2019.03.113.
[61] P. Bazylewski, R. Divigalpitiya, G. Fanchini, In situ Raman spectroscopy distinguishes between reversible and irreversible thiol modifications in L-cysteine, RSC Adv. 7 (2017) 2964–2970, https://doi.org/10.1039/c6ra25879d.
[62] M. Larsson, J. Lindgren, Analysis for glutathione and immunoglobulin G inside chromatographic beads using surface-enhanced Raman scattering spectroscopy, J. Raman Spectrosc. 36 (2005) 394–399, https://doi.org/10.1002/jrs.1304.
[63] C.K. Kwon, M.S. Kim, K. Kim, Raman spectroscopy of cyclohexanethiol adsorbed on a silver surface, J. Raman Spectrosc. 20 (1989) 575–580, https://doi.org/10.1002/jrs.1250200905.
[64] R.L. Frost, K.L. Erickson, Near-infrared spectroscopy of stitchtite, iowaite, desautelsite and arsenate exchanged takovite and hydrotalcite, Spectrochim. Acta Part A. 61 (2005) 51–56, https://doi.org/10.1016/j.saa.2004.03.011.
[65] R.L. Frost, H.J. Spratt, S.J. Palmer, Infrared and near-infrared spectroscopic study of synthetic hydrotalcites with variable divalent/trivalent cationic ratios, Spectrochim. Acta Part A. 72 (2009) 984–988, https://doi.org/10.1016/j.saa.2008.12.018.
[66] M. Mora, M.I. López, C. Jiménez-Sanchidrián, J.R. Ruiz, MIR and NIR spectroscopy of sol-gel hydrotalcites with various trivalent cations, J. Sol-Gel Sci. Technol. 55 (2010) 59–65, https://doi.org/10.1007/s10971-010-2213-x.
[67] M. Mora, M.I. López, C. Jiménez-Sanchidrián, J.R. Ruiz, Study of organo-hybrid layered double hydroxides by medium and near infrared spectroscopy, Spectrochim. Acta Part A. 78 (2011) 989–995, https://doi.org/10.1016/j.saa.2010.12.013.
[68] R.L. Frost, Z. Ding, J.T. Kloprogge, The application of near-infrared spectroscopy to the study of brucite and hydrotalcite structure, Can. J. Anal. Sci. Spectrosc. 45 (2000) 96–101.
[69] X. Zheng, C. Duan, J. Shen, X. Duan, Determination of reduced glutathione by spectrophotometry coupled with anti-interference compensation, Anal. Methods. 7 (2015) 5006–5011, https://doi.org/10.1039/c5ay00825e.
[70] G. Kalaiyarasan, A.V. Narendra Kumar, C. Sivakumar, J. Joseph, Electro-generated reactive oxygen species at Au surface as an indicator to explore glutathione redox chemistry and quantification, Electrochem. Commun. 56 (2015) 29–33, https://doi.org/10.1016/j.elecom.2015.03.021.
[71] X. Huang, J. Chen, H. Yu, S. Peng, R. Cai, Q. Yan, H.H. Hng, Immobilization of plant polyphenol stabilized-Sn nanoparticles onto carbon nanotubes and their application in rechargeable lithium ion batteries, RSC Adv. 3 (2013) 5310–5313, https://doi.org/10.1039/c3ra00139c.
[72] R. Stevens, L. Stevens, N. Price, The stabilities of various thiol compounds used in protein purifications, Biochem. Educ. 11 (1983) 70, https://doi.org/10.1016/0307-4412(83)90048-1.
[73] M. Aruga, S. Awazu, M. Hanano, Kinetic studies on decomposition of glutathione. I. Decomposition in solid state, Chem. Pharm. Bull. 26 (1978) 2081–2091, https://doi.org/10.1248/cpb.26.2081.